Assessment of Classical and Extended Messinger Models for Modeling Rotorcraft Icing Phenomena

Jeewoong Kim and Lakshmi Sankar
School of Aerospace Engineering, Georgia Tech, Atlanta, GA, USA

Richard E. Kreeger
NASA Glenn Research Center, Cleveland, OH, 44135, USA

Abstract

Numerical studies have been performed to systematically assess the difference between the classical and extended Messinger model for ice accretion. A number of 2-D steady airfoil, 2-D oscillating airfoil, and 3-D rotor configurations have been studied from the ice accretion perspective. A suite of tools including a grid generator, flow solver, droplet convection model solver and an ice accretion modeling tool have been developed and coupled to each other using open I/O standards (PLOT3D format). The ice accretion is modeled using a classical Messinger model available within NASA LEWICE3D solver, and compared with an extended methodology developed in-house. Numerical results are presented and compared with experimental data for a variety of geometries of interest to rotorcraft industry.

1. Introduction

Modern helicopters, civilian and military alike, are expected to operate in all weather conditions. Ice accretion adversely affects the safety and availability of helicopters because of the rapid rise in torque and power with ice accretion. Equipping the rotor blades with built-in heaters greatly increases the cost of the helicopter and places further demands on the engine. The safety of the vehicle is also compromised due to ice shedding events, and the onset of abrupt unexpected stall phenomena attributable to ice formation. Given the importance of understanding the effects of icing on rotorcraft performance and certification, considerable work has been done over the past two decades on the development of analytical and empirical tools, accompanied by high quality wind tunnel and flight test data. For pioneering research efforts in this area, the reader is referred to Ref. [1-12].

Because it is very expensive and time consuming to test and certify a helicopter for its entire range of operating conditions, it is customary to use icing tunnel test data for benchmark configurations, coupled with computational simulations for such configurations, validate the prediction methodologies. These methodologies with additional empirical corrections may subsequently be used to screen and reduce the number of flight test operating conditions. A coordinated effort has been under way to collect such data and develop computational tools. This effort is being done under the support of NASA Research Agreements (NRA), industry-university consortiums, and the Vertical Lift Research Centers of Excellence at Georgia Tech and Penn State. The present researchers are developing advanced tools for modeling ice accretion [13-15] that build on and complement LEWICE. Validation of these tools requires high quality data for ice shapes and associated airloads. An excellent set of test data is available from NASA Glenn for a variety of configurations [16-18].

The success of any ice accretion and growth calculation depends on an accurate estimate of the transition location which determines the surface heat transfer coefficient. The ice accretion is also influenced by the assumptions and empiricism within the mass balance and thermodynamic analyses. Many analyses, including the NASA LEWICE solver [16-18] employ the classical Messinger's model [19]. Extensions to the classical Messinger model have been proposed by Myers [20, 21]. These extensions have been evaluated by Ozgen et al. [22] for 2-D multi-element airfoils.

While the classical and extended models both have the same physical foundation, they differ considerably from each other in the way the boundary layer growth, transition location determination, and surface skin friction are treated. These methods also differ substantially in the way the heat and mass balance equations are modeled. The objective of the present study is to systematically assess the differences between the industry standard ice accretion analyses such as LEWICE and the ice accretion models based on the extended Messinger model. This is being done through a number of simulations for 2-D stationary airfoils, 2-D oscillating airfoils, and a Bell helicopter tail rotor.

2. Computational Methodologies

Current state of the art computational methodologies for modeling aircraft and rotorcraft icing follow the present approach.

1. The external aerodynamics of the clean, un-iced configuration is first modeled.
2. The velocity field from the computations is fed into a Lagrangian particle trajectory analysis, or an Eulerian droplet convection model, to determine the collection efficiency. This is a measure of the amount of water that enters the viscous layer close to the surface with a possibility of subsequent freezing.
3. The surface pressure distribution is next used to model the boundary layer growth and compute the surface skin friction distribution.
4. Reynolds analogy is next invoked to convert the surface skin friction distribution to the surface heat transfer rate.
5. A finite volume analysis of the conservation of water mass and energy is next done within the viscous layer near the solid surface. This ice growth in time is computed, with or without heating within the solid surface underneath.
6. At selected time levels, the resulting ice shape is added to the solid surface to establish an iced configuration.

Steps 1-5 are repeated as often as needed until the total time of ice accretion is reached. Figure 1 shows details of this process.

2-1. CFD solvers

The 2-D analyses in this work were done using a 3-D Reynolds-Averaged compressible Navier-Stokes solver called GENCAS (Generic Numerical Compressible Airflow Solver), [23, 24]. This analysis accepts 2D or 3D structured multi-block grids. The inviscid fluxes at the control volume faces are computed using Roe's Flux difference splitting scheme or the AUSMPW+ upwind schemes are available. The calculations are advanced in time using 1st or 2nd order implicit schemes. At each time step, the coupled non-linear equations are iteratively solved using a Newton-Raphson scheme. The system of linearized equations at each of the Newton-Raphson steps is solved using the LU Symmetric Gauss-Seidel scheme. Additionally, 2nd/4th order explicit Runge-Kutta schemes are available for time marching. For higher order accuracy, 3rd order MUSCL, 5th order and 7th order WENO cell interface reconstruction methods may be selected as a

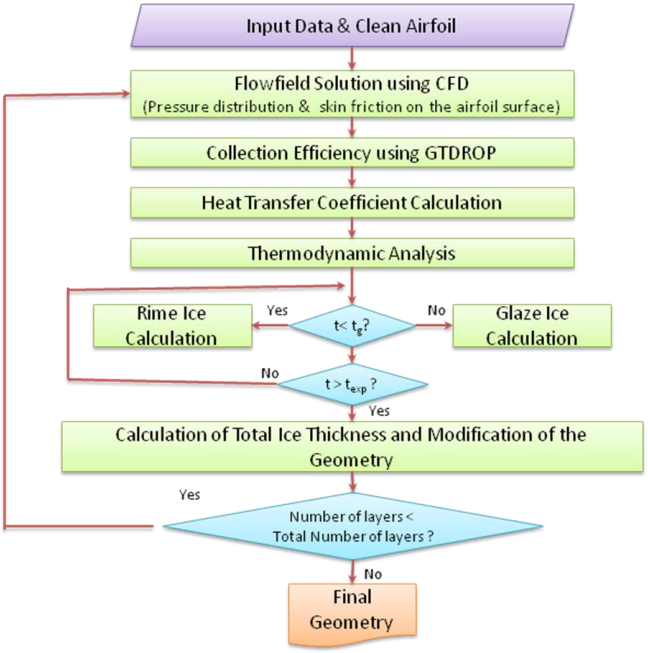

Figure 1. Overview of the Ice Accretion Analysis.

user input. A number of one-equation and two-equation turbulence models are available for modeling the eddy viscosity.

The 3-D simulations for the Bell tail rotor were computed using another flow solver called GT-Hybrid [25], a finite volume based three-dimensional unsteady viscous compressible flow solver. This analysis performs the costly Navier-Stokes calculations only in the immediate vicinity of the rotor blades. Away from the rotor, the vortex wake is captured using a Lagrangian approach. This hybrid approach allows for an accurate and economical modeling of viscous features near the blades, and an accurate "non-diffusive" modeling of the trailing wake in the far field. Figure 2 shows a schematic of the Hybrid method employed in GT-Hybrid, depicting the Navier-Stokes domain around the blade-region, the wake captured inside the near-blade Navier-Stokes domain, and the portion of the wake which is modeled as a Lagrangian free wake.

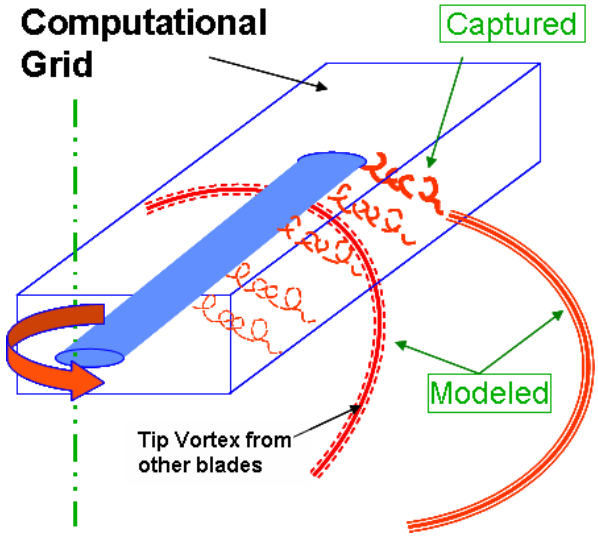

Figure 2. A Schematic View of the Hybrid Method.

The influence of the trailed vortices from the wake model on the blade aerodynamics is computed by appropriately specifying the vortex-induced velocities at the far field boundary of the Navier-Stokes domain, neglecting the contribution of the elements captured within the CFD volume grid.

2-2. Droplet Solver

Once the flow field is computed, the next step is to compute the volume fraction of the water droplets and the droplet velocity at the same nodes of the discrete domain where the flow variables of air are known. An in-house analysis called GTDROP [14] that is based on Eulerian approach is used. In this method, the average water droplet properties within a control volume are solved instead of tracking individual particles. This physical approach has several advantages over the Lagrangian approach. These include improved quality of the solution, the ability to model unsteady flows over bodies in relative motion, and the automated treatment of shadow zones around the rotor where there is no impingement. The interaction between the air particles and the droplets occurs through a drag force exerted by the mean flow on the particles. The presence of the droplet flow field is, however, not felt by the mean flow field solver, and the droplets are treated as a passive scalar field. When the air flow is steady, the CFD analysis may be computed a priori and used in the droplet solver. If the flow is unsteady, the droplet analysis should be done once every time step, after the mean flow properties are computed.

The governing equations for the conservation of mass and momentum of the droplets are written as follows:

$$\frac{\partial \alpha}{\partial t} + \nabla \cdot (\alpha u_i) = 0 \qquad (1)$$

$$\frac{\partial u_i}{\partial t} + u_i \cdot \nabla u_i = \frac{C_D \,\mathrm{Re}_d}{24K}(u_a - u_i) + \left(1 - \frac{\rho_a}{\rho}\right)\frac{1}{Fr^2} g_i \qquad (2)$$

Here, α is the non-dimensionalized volume fraction of water and u_i is the non-dimensional velocity of droplets.

Additionally, u_a is the non-dimensionalized velocity of air; ρ and ρ_a are the density of water and air, respectively; g_i, is the gravity vector; $F_r = U_\infty / \sqrt{Lg}$ is the Froude number; U_∞ is the speed of air at freestream; L, is the characteristic length (typically the airfoil chord length); $K = \rho d^2 U_\infty / 18 L\mu$, is an inertia parameter; and, μ is the dynamic viscosity of air.

The drag coefficient is defined as

$$C_D = \frac{24}{\mathrm{Re}_d}\left(1 + 0.15\,\mathrm{Re}_d{}^{0.687}\right) \qquad \mathrm{Re}_d \le 1000$$
$$C_D = 0.4 \qquad \mathrm{Re}_d > 1000 \qquad (3)$$

with,

$$\mathrm{Re}_d = \frac{\rho_a d U_\infty |u_a - u_i|}{\mu}$$

Equations (1) and (2) are recast in finite volume form using divergence theorem. A first order upwind scheme is employed for computing the mass and momentum flux at the faces of the control volume. An implicit time marching algorithm is employed. Mean flow quantities are lagged by one time step compared to particle velocity and volume fraction. The resulting system of banded linear equations is solved using an approximate factorization scheme.

2-3. Ice Accretion Solver

The present studies were conducted using LEWICE [26] which employs the classical Messinger model, and an in-house methodology developed by the present researchers that employs the extended Messinger model.

2-3-1. LEWICE

LEWICE [26], developed by the NASA Glenn Research Center, has been used by literally hundreds of users in the aeronautics community for predicting ice shapes, collections efficiencies, and anti-icing heat requirements. LEWICE consists of four major modules. The first module is flow field calculation using a panel method, developed by Hess and Smith [27]. The second module is a particle trajectory and impingement calculation using a Lagrangian approach by Frost et al [28]. Thermodynamic and ice growth calculation is done in a third module. An integral boundary layer method is used to determine the skin friction and the local convective heat transfer coefficient. Finally, the classical Messinger model [19] is for ice accretion thermodynamic analysis. LEWICE also has capability for de-icing and anti-icing analyses. All the modules have been seamlessly integrated. The analysis is robust and is capable of modeling 2-D and 3-D configurations ranging from simple airfoils to a complete aircraft configuration.

2-3-2. Extended Messinger Model

The extended Messinger Model [20,21] is based on the standard method of phase change or the Stefan condition [29], similar to the Messinger [19] energy balance in the form of a differential equation. The Stefan problem consists of four equations: heat equations in the ice and water layers, corresponding mass balance equations, and a phase change or Stefan condition at the ice/water interface. Figure 3 shows some of the details of the extended Messinger's model in one-dimension. The difference relative to the original Messinger model is that the extended Messinger model requires knowledge of the temperature gradients within each layer. The heat equations in the ice and water layer may however be analytically and economically solved, because of their simple forms.

An ice accretion code has been developed based on the extended Messinger formulation shown in Figure 3, with additional details given in Ref. 20 and 21. The boundary layer analysis is done by Thwaites' method for the laminar flow region, and Head's method for the turbulent flow region. Instead of using empirical skin friction equation, skin friction coefficient from CFD simulation is used for the boundary layer and the thermodynamic analysis. Transition location is determined by Von Doenhoff criterion, $Re_k > 600$, where Re_k is the Reynolds number based on the roughness height and the local edge velocity.

3. Results and Discussions

In this section, a number of ice accretion simulations are presented with the classical and extended Messinger models for ice accretion.

3-1. Stationary Airfoil

Ref. 16 contains a rich set of validation data for ice accretion over a NACA0012 airfoil. A specific condition called runs 308 has been modeled using the present suite of tools. Table 1 shows the flow conditions, closer to glaze ice conditions. GENCAS is used to obtain flow field data. In the CFD simulation, Roe scheme with a 3rd order MUSCL reconstruction is used for flux calculations. A temporally first order implicit LUSGS scheme is used for marching in time. Spalart-Allmaras (SA) is used to compute eddy viscosity distributions. A structured C-type mesh (397 x 101) is used.

During the ice accretion phase of the simulation, a multi-step approach is used with a time step of 57.75 sec. Figure 4 shows the computed ice shape. Three different simulations are performed. LEWICE means a stand-alone mode simulation (case 1). The other two cases use data from CFD simulation and Eulerian droplet simulation in order to calculate ice growth. LEWICE (case 2) and ice accretion code using the extended Messinger model (case 3) are used. All simulations show an under-prediction of the horn shape formed over the upper part of the airfoil. Although case 1 and 2 show good agreement near the stagnation point, the location of upper horn is shifted to downstream. While case 3 predicted the location of upper horn fairly well, ice thickness near leading edge is overpredicted.

3-2. Oscillating Airfoil

Ice growth simulations on an oscillating airfoil, an SC2110 test section tested at NASA Glenn Research Center [30] have been performed for a specific condition called runs 308. Table 2 gives the test conditions for this case. GENCAS is also used to obtain flow field data. In the CFD simulation, same options used in stationary airfoil case are used.. A structured C-type mesh (397 x 101) is used. A fine grid study (588 x 121) was also done, and produced very similar results.

The ice accretion event is divided into a few time steps with data exchanges occurring before each step rather than continuously. Following time-step sensitivity studies, 4 steps per cycle, as shown in Figure 5, are used. At each of these angles of attack, the collection efficiency was computed using the CFD results. The collection efficiency and the surface pressure data were fed into the ice accretion codes, and ice was allowed to grow for 75 seconds at each of the 8 time levels, for a total of 600 seconds. Figure 6 shows the computed ice shape. Comparisons with experimental data and ice shape from Ref. 30 (Icemaker) are shown in Figure 6.

3-3. 3D Ice Accretion for a Teetering Rotor

Extensive rotor blade ice tests have been done in NASA Glenn's Icing Research Tunnel (IRT) in September 2013 [31]. In the present work, ice growth simulations have been performed for just one of the numerous test conditions.

The model rotor is a production of Bell Helicopter Model 206B tail rotor blade with heater blankets bonded to the blade surface. The rotor is a two-bladed teetering rotor with a δ_3 of 45°. The rotor radius is 32.6", a chord of 5.3" and has rectangular blade with NACA0012 airfoil.

One of test conditions, Run53, is selected as a baseline case. Table 3 shows the corresponding test conditions. The blade motion (flapping angle) is computed from a coupled CFD / Flapping Dynamics analysis of the clean rotor. Flapping angles of blade are recomputed after each CFD simulation. The calculations are redone using the new flapping angles. The simulations continued until the hub roll and pitching moments are zeroed out. Figure 7 shows flowchart of the CFD / Flapping Dynamics analysis.

Table 1. Test Conditions for Run 308.

Air speed (m/sec)	102.8
Angle of Attack (Deg.)	3.5
LWC (g/m^3)	1.0
Drop (μm)	20
Temperature (K)	262.04
Time (Min)	3.85
Airfoil	NACA0012
Chord (in)	21

Table 2. Test Conditions for Run 61.

Air speed (knot)	150
Angle of Attack (Deg.)	5 ± 6
LWC (g/m^3)	1.0
Drop (μm)	22
Temperature (K)	259.15
Time (Min)	10
Airfoil	SC2110
Chord (in)	15

Table 3. Test Conditions for Run53.

Forward Velocity (knot)	60
RPM	1200
LWC (g/m^3)	0.5
Drop (μm)	15
Temperature (K)	263.15
Time (Min)	3
Collective (Deg.)	2

Prior to the ice accretion simulation, performance predictions for clean rotor (Run 84) have been done to validate the Coupled CFD / Flapping Dynamics method. A C-H grid, 131 (chordwise) x 70(spanwise) x 45 (normal), was used. Run 84 represents a dry air test for a sweep of collective pitch angles 0°, 2°, 5°, 8°, and 10° with each angle sustained for around 20 seconds. The tunnel was run at an ambient temperature of -10° C (14° F) and 60 kts. The predicted thrust and power are compared with measured values in Fig. 8 and 9. Thrust and power are compared after every iteration of the Coupled CFD / Flapping Dynamics analysis, respectively denoted as Itn-0 through Itn-2. While the predicted results are not exactly equivalent to the experiment, the consistent trend in thrust and power validates the Coupled CFD / Flapping Dynamics method.

The predicted flowfield solutions from CFD simulation were fed into an Eulerian droplet model and the two ice accretion codes in order to get the ice shape. A multi-step approach is used with a time step of 57.75 sec. The ice was accreted at four different azimuthal locations (Ψ = 0°, 90°, 180°, 270°). Unsteady flow field data for the clean rotor was used to compute the collection efficiencies at each azimuthal location.

Figure 10 shows the comparison of predicted ice shape using two ice accretion codes (LEWICE and Extended Messinger model) at the selected radial locations 37% R, 50% R, 61% R, 74% R, and 86% R, and 98% R. Ice shapes predicted from both approach are smooth and rounded. Marginal difference in ice shape is seen at the inboard between LEWICE and Extended Messinger model. Predicted ice shapes from both approaches are close to experimental ice shape at the inboard region. Ice shapes start to differ towards blade tip. As seen in the 2D cases, the Extended Messinger model predicts thicker ice near the leading edge of airfoil. The predicted maximum ice thickness from the Extended Messinger model is closer to experiment [31].

Performance predictions using predicted ice shape from the Extended Messinger model have been done to investigate the effect of ice formation on rotor performance. The grid density for the clean rotor and iced rotor simulations are comparable, with the same number of nodes in the wrap-around, normal, and radial directions with comparable grid spacings. Other options (temporal and spatial discretization, turbulence models) were also kept the same in the clean and iced rotor simulations.

Predicted thrust and power of iced rotor have also been compared with measured values (unpublished data). The power is increased by 35% and thrust is decreased by 16% compared to clean rotor. The computed and measured thrust values are in reasonable agreement. The predicted power is much lower than experiment. One of possible reason for this discrepancy is the lack of surface roughness modeling in the CFD solver. The performance degradation of the iced rotor compared to clean rotor is only qualitatively captured.

4. Summary and Recommendations

Ice accretion calculations have been done using the classical and extended Messinger model for a 2-D stationary airfoil, 2-D oscillating airfoil, and 2-bladed teetering rotor. In the 2D cases, the Extended Messinger model predicts thicker ice near the leading edge of airfoil. For 3-D rotor ice accretion, marginal difference in ice shape is seen at the inboard between two approaches and shows good agreement with experimental ice shape. Although the actual values of rotor performance are not predicted, performance degradation due to the ice is captured from modern state of the art method.

Acknowledgments

This project was funded by the U. S. Army under the Vertical Lift Research Center of Excellence (VLRCOE) program managed by the National Rotorcraft Technology Center, Aviation and Missile Research, Development and Engineering Center under Cooperative Agreement W911W6-06-2-0004 between Georgia Institute of Technology and the U. S. Army Aviation Applied Technology Directorate. Dr. Mahendra Bhagwat is the technical monitor. The authors would like to acknowledge that this research and development was accomplished with the support and guidance of the NRTC. The views and conclusions contained in this document are those of the authors and should not be interpreted as representing the official policies, either expressed or implied, of the Aviation and Missile Research, Development and Engineering Center or the U.S. Government.

$$\frac{dT}{dt} = \frac{k_i}{\rho_i c_i}\frac{\partial^2 T}{\partial z^2}$$ Heat equation in the ice

$$\frac{d\theta}{dt} = \frac{k_w}{\rho_w c_w}\frac{\partial^2 \theta}{\partial z^2}$$ Heat equation in the water

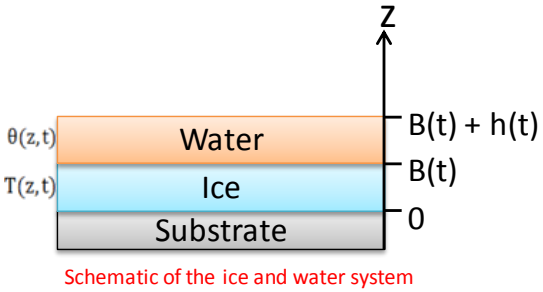

Schematic of the ice and water system

$$\rho_i \frac{dB}{dt} + \rho_w \frac{dh}{dt} = \rho_a \beta V_\infty + \dot{m}_{in} - \dot{m}_{e,s}$$ Mass balance

$$\rho_i L_F \frac{dB}{dt} = k_i \frac{\partial T}{\partial z} - k_w \frac{\partial \theta}{\partial z}$$ Stefan condition at the ice / water interface

T, θ : Temperature t : time k_i, k_w : thermal conductivity of ice and water

ρ_i, ρ_w, ρ_a: density of ice, water and air c_i, c_w : specific heat of ice and water

B, h : thickness of ice and water layers $\rho_a \beta V_\infty$: impinging mass flow rate for a control volume

L_F: latent heat of solidification of water $\dot{m}_{in}$: runback mass flow rate for a control volume

$\dot{m}_{e,s}$: evaporating (or sublimating) mass flow rate for a control volume

Figure 3. Details of the Extended Messinger Model in One Dimension.

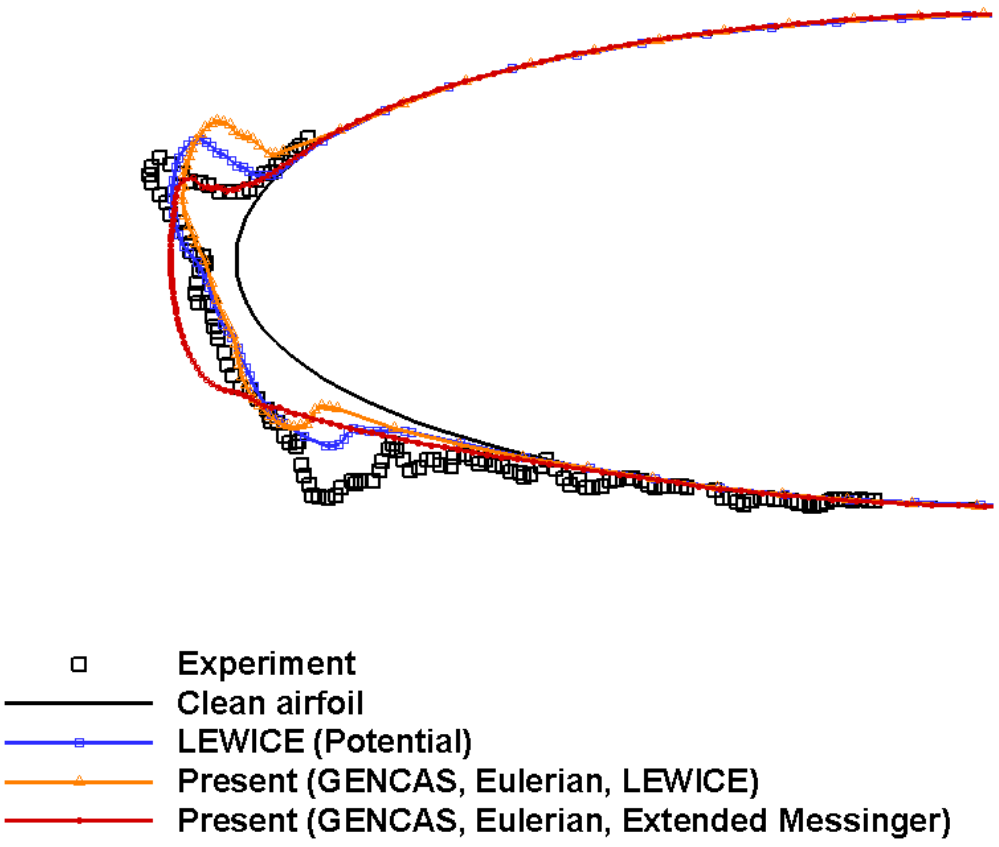

Figure 4. Predicted ice shape for NACA0012 (Run 308).

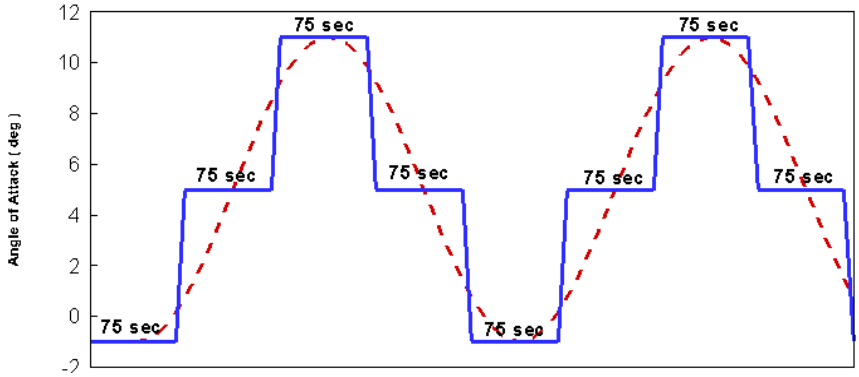

Figure 5. Characterization of the airfoil angle of attack.

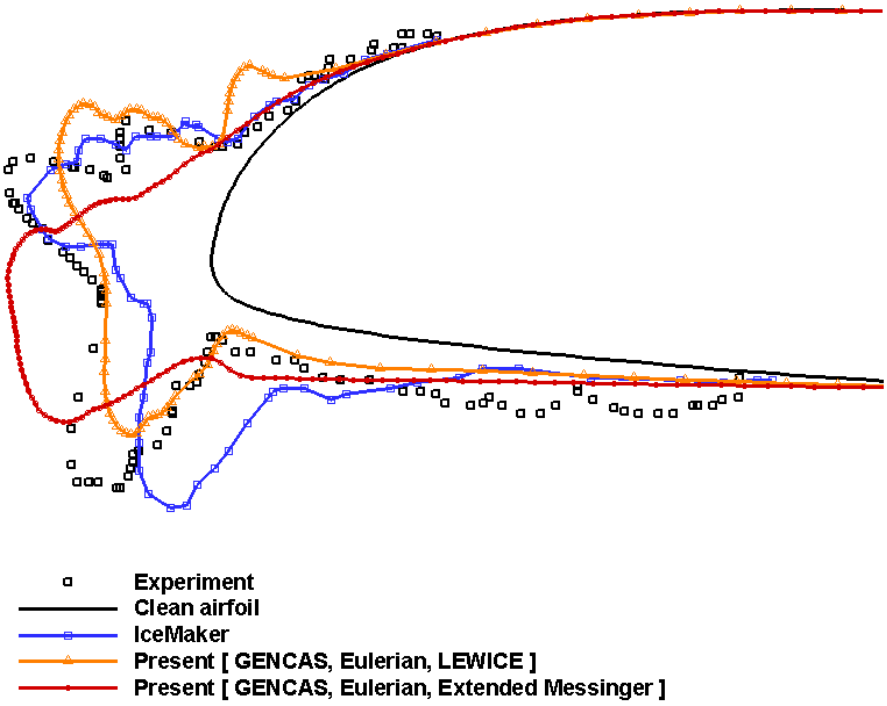

Figure 6. Comparisons of ice shape for an oscillating SC 2110 airfoil.

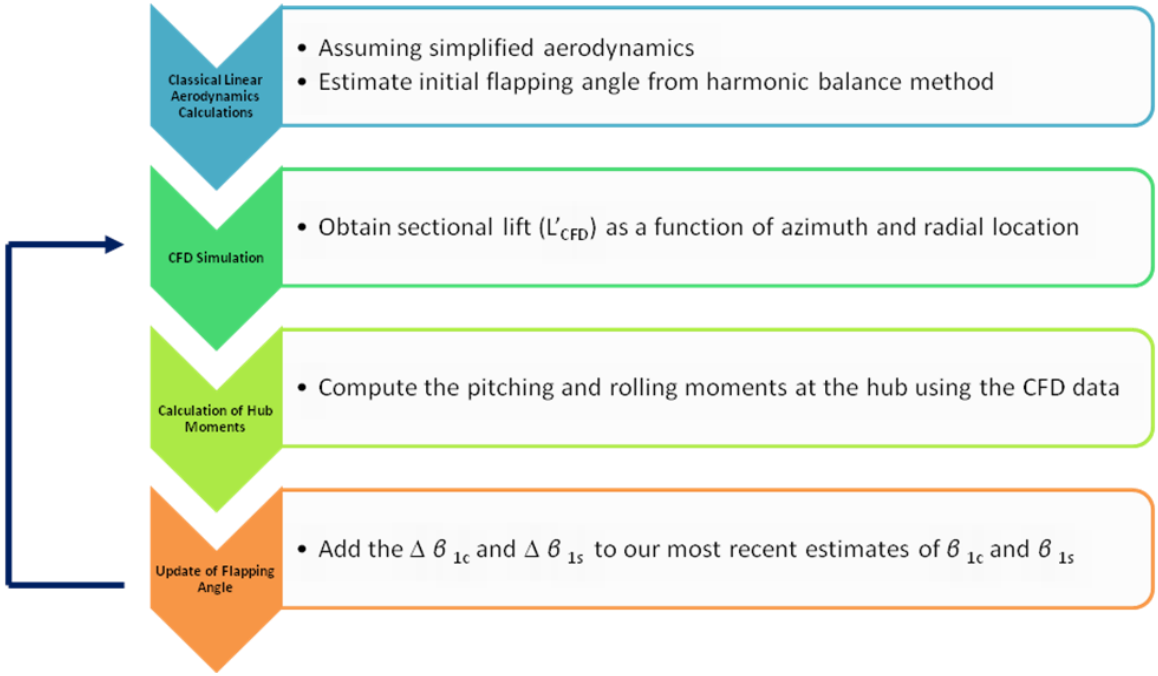

Figure 7. Flowchart of the CFD / Flapping Dynamics analysis.

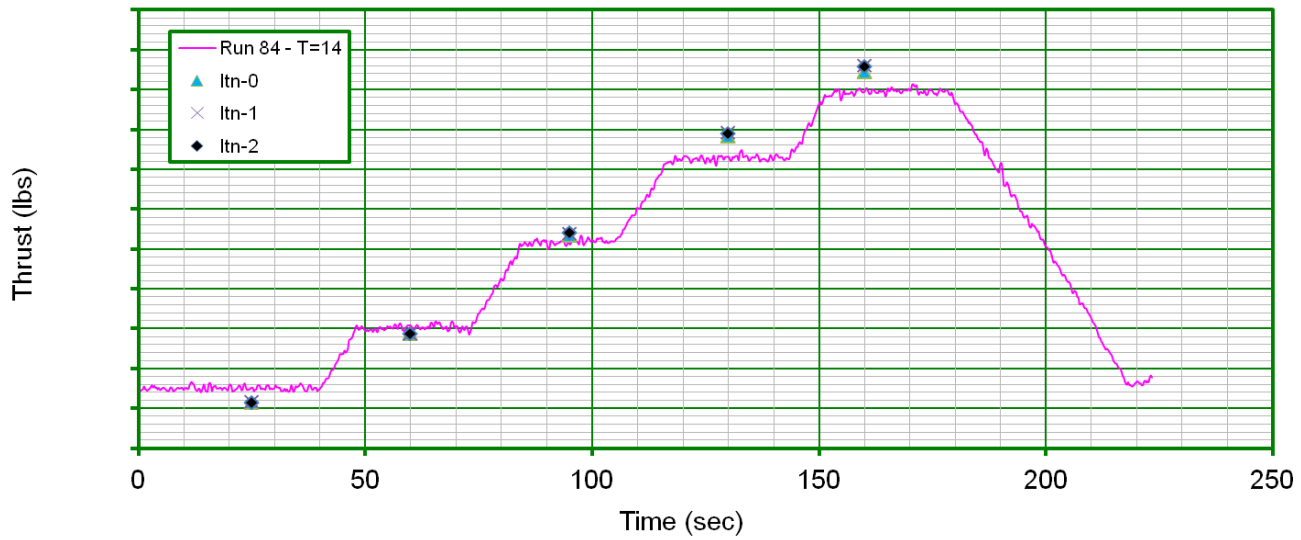

Figure 8. Comparison of experimental thrust values (Run 84) with CFD / Flapping Dynamics analysis for collective sweep 0°, 2°, 5°, 8°, 10°

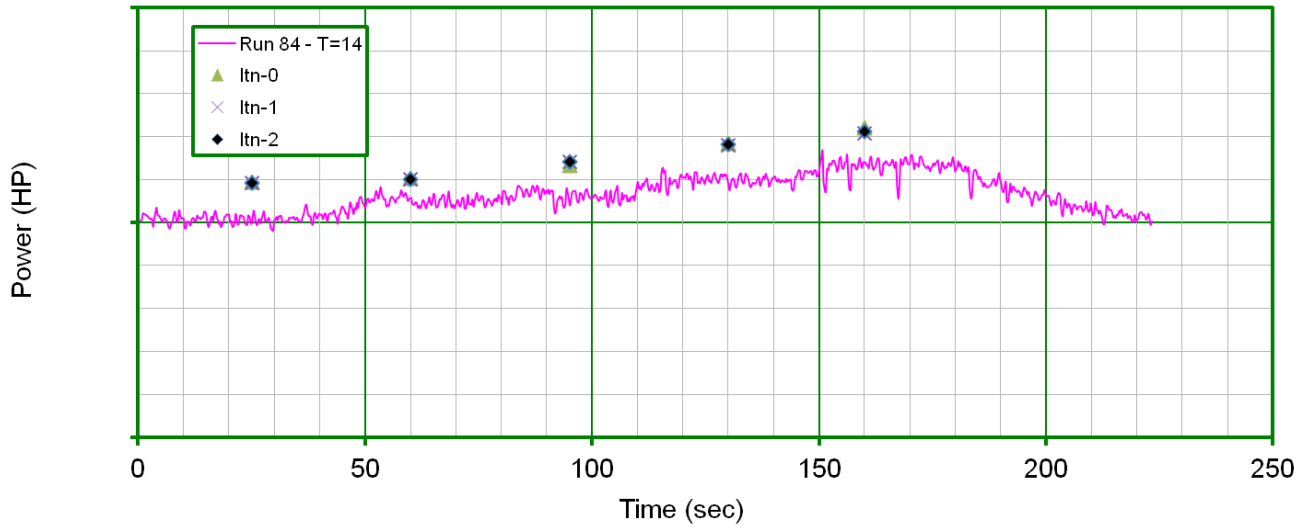

Figure 9. Comparison of experimental thrust values (Run 84) with CFD / Flapping Dynamics analysis for collective sweep 0°, 2°, 5°, 8°, 10°.

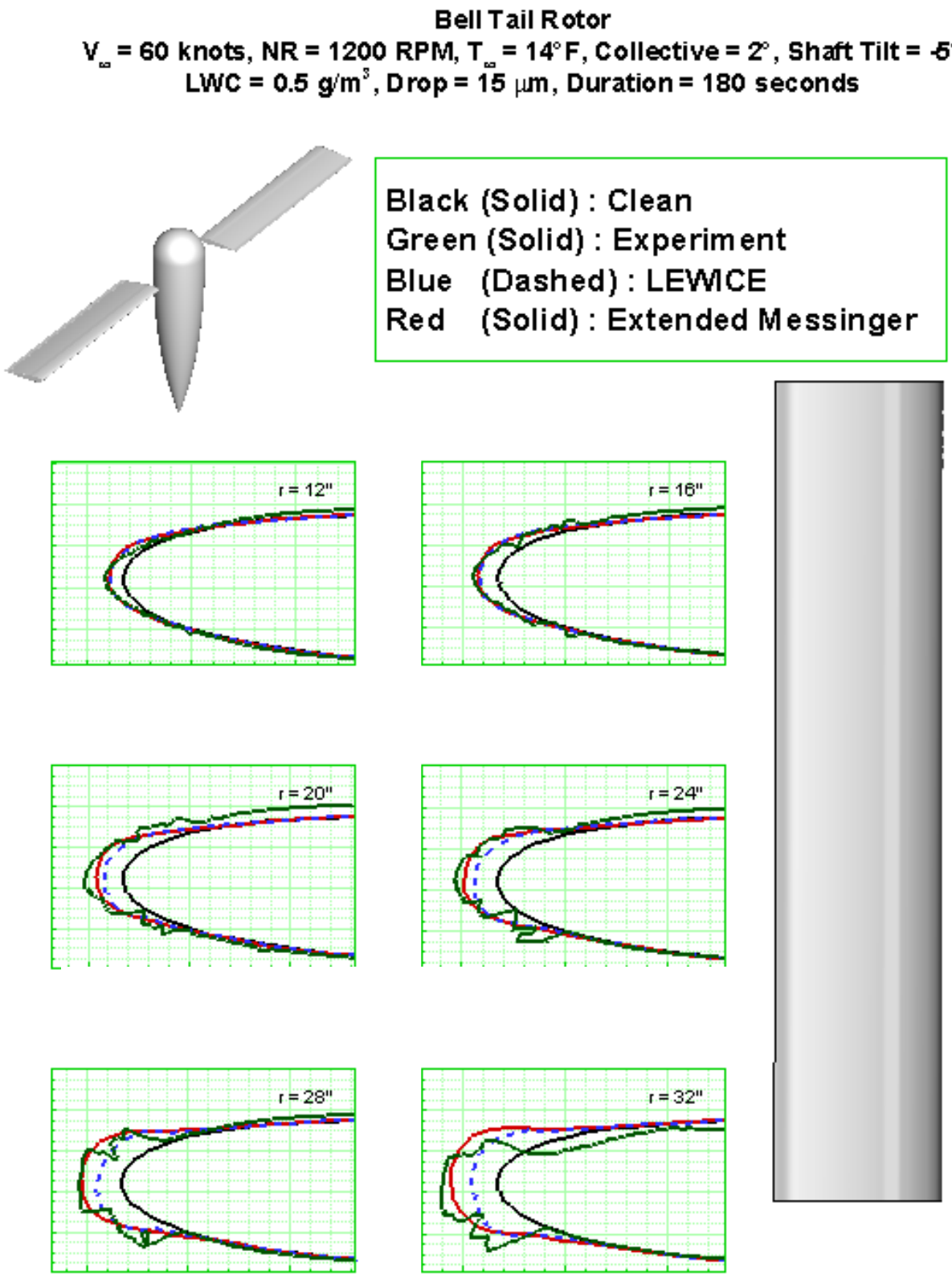

Figure 10. Comparisons of ice shape for a Bell Tail Rotor.

REFERENCES

[1] Bell, J.D., “Icing at the McKinley Climatic Laboratory, an Update of the New Icing Capability Project,” AIAA Paper 2004-0735, January 2004.

[2] Ward, R.N. et al, “Climatic Laboratory Evaluation - Iranian Model 214A Helicopter,” Final Report for U.S. Army USAAEFA Project Number 74-32, August 1974.

[3] Flemming, R.J. and Lednicer, D.A., “High Speed Ice Accretion on Rotorcraft Airfoils,” NASA Contractor Report 3910, August 1985.

[4] Flemming, R.J. and Saccullo, A., “Tests of a Model Main Rotor in the NASA Lewis Research Center Icing Research Tunnel,” NASA Contractor Report 189071, December 1991.

[5] Britton, R.K., “Ice Accretion Characteristics of a Model Rotor in the NASA Lewis Icing Research Tunnel,” AHS International Icing Symposium 1995 Proceedings, September 1995.

[6] Flemming, R.J., “Performance Characteristics of a Model Rotor in Icing,” AHS International Icing Symposium 1995 Proceedings, September 1995.

[7] Flemming, R.J., Britton, R., and Bond, T., “Role of Wind Tunnels and Computer Codes in the Certification and Qualification of Rotorcraft for Flight in Forecast Icing,” NASA Technical Memorandum 106747, October 1994.

[8] Flemming, R.J., Murty, H., Michael Papadakis, and See-Ho Wong, “Design, Fabrication, and Testing of Simulated Ice Shapes for the S-92A Helicopter,” AIAA Paper 2004-0736, January 2004.

[9] “Title 14 of the Code of Federal Regulations, Part 29: Airworthiness Standards, Transport Category Rotorcraft” (date consistent with amendment and certification basis).

[10] Federal Aviation Administration Advisory Circular AC 29-2C, “Certification of Transport Category Rotorcraft,” September 30, 1999.

[11] SAE ARD5906, “Ice Shape Measurements and Comparison Techniques Workshop,” 2003.

[12] Flemming, R. J., “The past twenty years of icing research and development at Sikorsky Aircraft,” AIAA-2002-0238 AIAA Aerospace Sciences Meeting and Exhibit, 40th, Reno, NV, Jan. 14-17, 2002.

[13] M. Nucci, J. Bain and L. Sankar, "Assessment of the Effects of Computational Parameters on Physics-based Models of Ice Accretion," 48th AIAA Aerospace Sciences Meeting, Orlando, FL, January 2010.

[14] J. W. Kim, D. P. Garza and L. N. Sankar, "Ice Accretion Modeling using an Eulerian Approach for Droplet Impingement," 51st AIAA Aerospace Sciences Meeting, Grapevine, Texas, January 2013.

[15] Bain, J., Sankar, L.N., Deresz, R., Egolf, T.A., Flemming, R.J., and Kreeger, R., “Effects of Icing on Rotary Wing Loads and Surface Heat Transfer Rates,” AIAA-2011-1100, 49th AIAA Aerospace Sciences Meeting including the New Horizons Forum and Aerospace Exposition, Orlando, Florida, Jan. 4-7, 2011.

[16] Wright, W. B., and Rutkowski, A., “Validation Results for LEWICE 2.0” [CD-ROM], NASA CR 1999208690, Jan. 1999.

[17] Wright, William B., “Validation Results for LEWICE 3.0,” NASA/CR-2005-213561; E-15007; AIAA Paper 2005-1243.

[18] Wright, W. B., and Rutkowski, A., “Validation Results for LEWICE 2.0” [CD-ROM], NASA CR 1999208690, Jan. 1999.

[19] Messinger, B. L., “Equilibrium Temperature of an Unheated Icing Surface as a Function of Air Speed,” Journal of the Aeronautical Sciences, Jan.1953, pp.29–42.

[20] Myers TG , “Extension to the Messinger model for aircraft icing,” AIAA Journal, Vol. 39, No. 2, 2001, pp. 211–218.

[21] Myers TG, Charpin JPF, Thompson CP (2002), "Slowly accreting ice due to supercooled water impacting on a cold surface," Phys Fluids 14(1):240–256.

[22] Ozgen S., Canibek M., “Ice accretion simulation on multi-element airfoils using extended Messinger model,” Heat and Mass Transfer, Vol. 45, 2009 pp. 305-322.

[23] Min, B. Y. and Sankar, L. N., “Enhancements to a Hybrid Navier-Stokes/Free Wake Method for Improved Prediction of Blade-Vortex-Interaction Phenomena,” AIAA 2009-3860, 27th AIAA Applied Aerodynamics Conference, San Antonio, Texas, June 22-25, 2009.

[24] Min, B. Y., Lee, W., Englar, R. and Sankar, L. N., “Numerical Investigation of Circulation Control Airfoils,” Journal of Aircraft, vol. 46, No. 4, pp. 1403-1410, 2009.

[25] N. Rajmohan, L. N. Sankar, O. Bauchau, B. Charles, S. Makinen and T. A. Egolf, "Application of hybrid methodology to rotors in steady and maneuvering flight," in AHS 64th Annual Forum, 2008.

[26] Wright, W. B., “User Manual for LEWICE Ver. 3.2,” NASA CR 214255, Cleveland, OH, 2008.

[27] J. L. Hess and A. M. O. Smith, "Calculation of potential flow about arbitrary bodies," *Progress in Aeronautical Sciences,* vol. 8, pp. 1-138, 1967.

[28] W. Frost, H. Chang, C. Shieh and K. Kimble, "Two-dimensional particle trajectory computer program," Interim Report for Contract NAS3-22448, 1982.

[29] Hill, J. M., *One-Dimensional Stefan Problems: An Introduction*, Longman Science Technical, Harlow, England, U.K., 1987, Chap. 1.

[30] Narducci, R. J. and Reinert, T., "Calculations of Ice Shapes on Oscillating Airfoils," SAE/AIAA/AHS International Conference on Aircraft and Engine Icing and Ground Deicing, SAE 2011-38-0015, 2011.

[31] Kreeger, Richard, E. And Tsao, Jen-Tsing, “Ice Shapes on a Tail rotor,” AIAA Paper 2014-2612, 6th AIAA Atmospheric and Space Environments Conference, Atlanta, GA, June 2014.

Copyright Statement